nature cell biology

Dynamic maintenance of asymmetric meiotic spindle position through Arp2/3-complex-driven cytoplasmic streaming in mouse oocytes

Kexi Yi[1], Jay R. Unruh[1], Manqi Deng[2], Brian D. Slaughter[1], Boris Rubinstein[1] and Rong Li[1,3,4]

Mature mammalian oocytes are poised for completing meiosis II (MII) on fertilization by positioning the spindle close to an actomyosin-rich cortical cap[1–3]. Here, we show that the Arp2/3 complex localizes to the cortical cap in a Ran-GTPase-dependent manner and nucleates actin filaments in the cortical cap and a cytoplasmic actin network. Inhibition of Arp2/3 activity leads to rapid dissociation of the spindle from the cortex. Live-cell imaging and spatiotemporal image correlation spectroscopy analysis reveal that actin filaments flow continuously away from the Arp2/3-rich cortex, driving a cytoplasmic streaming expected to exert a net pushing force on the spindle towards the cortex. Arp2/3 inhibition not only diminishes this actin flow and cytoplasmic streaming but also enables a reverse streaming driven by myosin-II-based cortical contraction, moving the spindle away from the cortex. Thus, the asymmetric MII spindle position is dynamically maintained as a result of balanced forces governed by the Arp2/3 complex.

Oocytes undergo two highly asymmetric meiotic divisions, giving rise to a large haploid egg and two much smaller polar bodies[4]. These asymmetric divisions require the meiotic spindle to be positioned closely to the cortical region where polar body extrusion occurs. The asymmetric spindle positioning in meiosis I (MI) is established through actin-dependent spindle migration to the cortex[5–7]. The meiotic chromatin then signals the assembly of a cortical domain, consisting of an actin cap surrounded by a ring of myosin-II, instrumental for polar body extrusion[8,9]. In MII, the second meiotic spindle assembles around the chromosomes already positioned near the cortex. In many vertebrate species including mammals, the oocyte may arrest in MII for hours to days awaiting fertilization[10], during which the asymmetric spindle position must be stably maintained. In asymmetrically dividing mitotic cells, the spindle position/orientation is usually accomplished by microtubules and their associated motors[11]; however, disrupting microtubules does not affect the subcortical location of MII chromatin[8]. Early and recent studies in mouse oocytes revealed a possible role for actin in maintaining MII spindle position asymmetry[12,13].

To assess the role of actin in MII spindle positioning, we incubated mouse oocytes with the available chemical inhibitors of the actin cytoskeleton, including latrunculin A (LatA), an inhibitor of actin polymerization[14], blebbistatin, inhibiting myosin-II ATPase activity[15], and CK-666 (ref. 16), an inhibitor of the Arp2/3 complex (actin-related protein 2/3 complex), an actin nucleator involved in cell motility and membrane trafficking[17]. Surprisingly, among these only CK-666 potently disrupted the subcortical spindle position. In $60.25 \pm 3.32\%$ of MII oocytes ($n = 68$) treated with 50 μM CK-666, the spindles were detached from the cortex (>1/3 oocyte radius away from the closest cortex, Fig. 1a,c), whereas 95.35% of control oocytes ($n = 51$) maintained a subcortically located spindle. To confirm that the effect of CK-666 was indeed due to inhibition of Arp2/3 complex activity, we injected MII oocytes with messenger RNA encoding two tandem CA (cofilin homology acidic region) domains (2CA) from N-WASP (neuronal Wiskott–Aldrich syndrome protein), an activator of the Arp2/3 complex[18]. CA binds to but does not activate the Arp2/3 complex, thus having a dominant-negative effect, expected to be enhanced by dimerization[19]. As a negative control, 2(CA^{W55A}), bearing the W55A mutation that demolishes the affinity with Arp2/3 (ref. 20), was used. 2CA induced a significant spindle positioning defect when compared with 2(CA^{W55A}) expressed at similar levels (Fig. 1c and Supplementary Fig. S1).

Video microscopy imaging showed that, within 5 min after the CK-666 addition, the spindle underwent directed movement towards the oocyte centre at an average speed of 0.39 ± 0.04 μm min^{-1} ($n = 17$; Fig. 1b and Supplementary Movie S1). As the cortical cap is rich in actin and myosin-II and the spindle movement induced by CK-666 was often accompanied by an apparent contraction of the cap region (see below), we investigated the effect of blebbistatin on this movement. Whereas

[1]Stowers Institute for Medical Research, 1000 East 50th Street, Kansas City, Missouri 64110, USA. [2]Department of Obstetrics and Gynecology and Reproductive Biology, Brigham and Women's Hospital, Harvard Medical School, Boston, Massachusetts 02115, USA. [3]Department of Molecular and Integrative Physiology, University of Kansas Medical Center, 3901 Rainbow Boulevard, Kansas City, Kansas 66160, USA.
[4]Correspondence should be addressed to R.L. (e-mail: rli@stowers.org)

Received 18 March 2011; accepted 13 July 2011; published online 28 August 2011; DOI: 10.1038/ncb2320

© 2011 Macmillan Publishers Limited. All rights reserved.

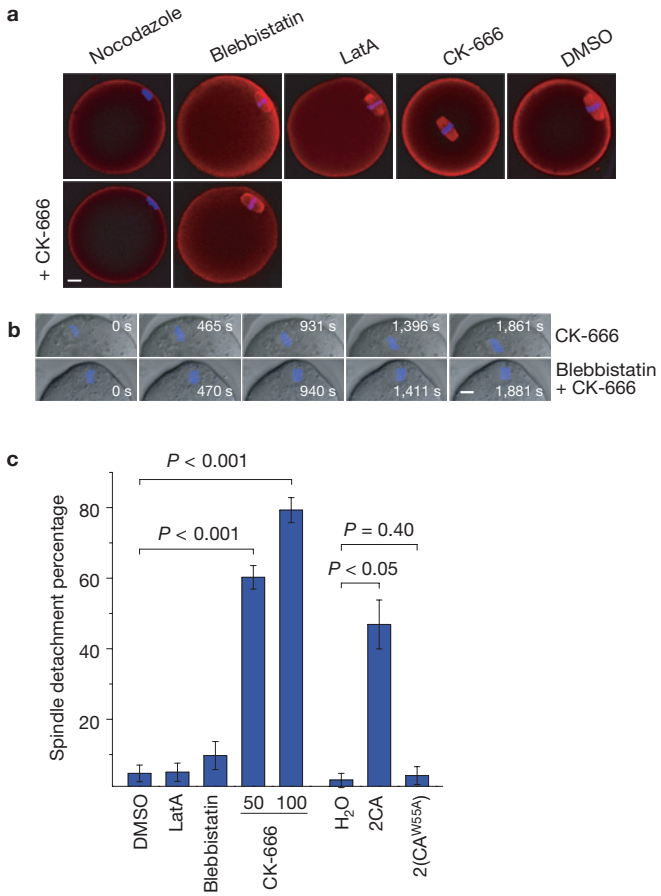

Figure 1 Inhibition of Arp2/3-complex activity disrupts asymmetric MII spindle position. (**a**) Representative images of MII spindle position after different drug treatments. The Arp2/3 inhibitor CK-666 (50 μM) induced spindle detachment from the cortex towards the cell centre. The four leftmost panels show the effects of blebbistatin and nocodazole on CK-666-induced spindle detachment. Scale bar, 10 μm. (**b**) Time-lapse imaging of chromosome movement in MII oocytes treated with 50 μM CK-666 with and without 100 μM blebbistatin. Scale bar, 10 μm. (**c**) Quantification of spindle detachment percentage after various treatments as indicated. Data are mean ± s.e.m. from three experiments, 22–52 oocytes per experiment.

blebbistatin alone had no effect on spindle position, it prevented spindle detachment from the cortex in the presence of CK-666 (Fig. 1a,b and Supplementary Movie S2), indicating that myosin-II contractility causes the spindle to move away from the cortex when the Arp2/3 complex is inhibited. This result also explains the apparent paradox that LatA treatment does not readily alter spindle position, as LatA disrupts both Arp2/3-nucleated actin assembly and contractile actomyosin structures. Interestingly, whereas nocodazol had no effect on meiotic chromosome position on its own, this treatment also prevented the chromosomes from detaching from the cortical cap on CK-666 incubation and the chromosomes seemed more tightly associated with the cortex (Fig. 1a).

Immunostaining with a polyclonal anti-Arp2 antibody showed localization of Arp2 to the cortical actin cap overlying the spindle (Fig. 2a). Cortical cap localization of Arp2/3 was further confirmed by expression of enhanced green fluorescent protein (eGFP)-tagged Arp3 through RNA injection (Fig. 2a). Immunostaining with an anti-N-WASP antibody also showed N-WASP localization to the actin cap (Supplementary Fig. S2a), whereas cortical localization of WAVE-type Arp2/3 activators was not detected (data not shown). N-WASP knockdown by morpholino injection (Supplementary Fig. S2b) disrupted Arp2 localization (Supplementary Fig. S2c) and also caused spindle detachment in 57.2% ($n = 53$) of the injected MII oocytes (Supplementary Fig. S2d). These data indicate that the N-WASP-stimulated actin nucleation activity of the Arp2/3 complex is required for the maintenance of the asymmetric positioning of the MII spindle.

Our previous work showed that meiotic chromatin, when positioned in proximity to the cortex of an MII oocyte, induces the formation of a cortical actin cap through Ras-related nuclear protein (Ran) GTPase signalling[8]. We therefore examined whether the Ran signal also regulates Arp2/3 complex localization and spindle position. MII oocytes were injected with a dominant-negative Ran protein, Ran^{T24N} (ref. 21). Ran^{T24N} disrupted asymmetric positioning of MII spindle in 70.97% ($n = 31$) of the injected MII oocytes, recapitulating the effect of Arp2/3 inactivation, whereas injection of wild-type Ran protein or buffer alone had no effect (Fig. 2b). Although the cortical localization of Arp2 was also disrupted in the Ran^{T24N}-injected oocytes where the spindle had moved away from the cortex, this may simply be due to the diminished chromatin signal to the cortex. To clarify this, nocodazole was added to the culture medium for Ran^{T24N}-injected oocytes because nocodazol prevented chromosome detachment from the cortex; however, Arp2 still delocalized from the cortical cap (Fig. 2c). Ran inhibition also disrupted the localization of N-WASP (Fig. 2c). Thus, Ran GTPase regulates N-WASP and Arp2/3-complex localization to the chromatin-proximal cortex.

We next examined the effect of Arp2/3 inhibition on actin organization. Most of the oocytes treated with CK-666 no longer retained the cortical actin cap, as expected considering the diminished chromatin signal after the spindle movement away from the cortex. However, even in those remaining oocytes with spindles still located subcortically after CK-666 treatment, the actin cap was significantly diminished, as revealed by phalloidin staining (Fig. 3a,b), while myosin-II remained associated with the same cortical region as a cap instead of a ring (Fig. 3a and Supplementary Fig. S3a). Inhibition of actin assembly in the cortical cap by CK-666 was also observed in nocodazole-treated oocytes where the chromatin stayed in close contact with the cortex (Fig. 3b). The same result was also confirmed by using the 2CA peptide (Fig. 3c,d). Disruption of N-WASP or upstream Ran signalling by Ran^{T24N} also led to the loss of the cortical actin cap (Supplementary Fig. S2c and Fig. 2c,d, respectively).

Recent work in MI mouse oocytes using live F-actin probes revealed the presence of dynamic cytoplasmic actin structures[22–24]. One such probe, UtrCH–GFP (the calponin homology domain of utrophin fused to GFP), was instrumental for the observation of an extensive cytoplasmic actin network connected with the MI spindle[25]. We expressed UtrCH–GFP in MII mouse oocytes and observed a similarly extensive F-actin network that was disrupted by LatA as well as by CK-666 treatment (Supplementary Fig. S4a) or 2CA expression (Supplementary Fig. S4b), indicating that the Arp2/3 complex is also responsible for the assembly of this actin network. The UtrCH–GFP-labelled actin network can also be visualized by injection with rhodamine–phalloidin (Supplementary Fig. S4b). Lifeact–GFP, another useful F-actin probe[26], stained only the actin cap but not the cytoplasmic actin network (data not shown), indicating that

© 2011 Macmillan Publishers Limited. All rights reserved.

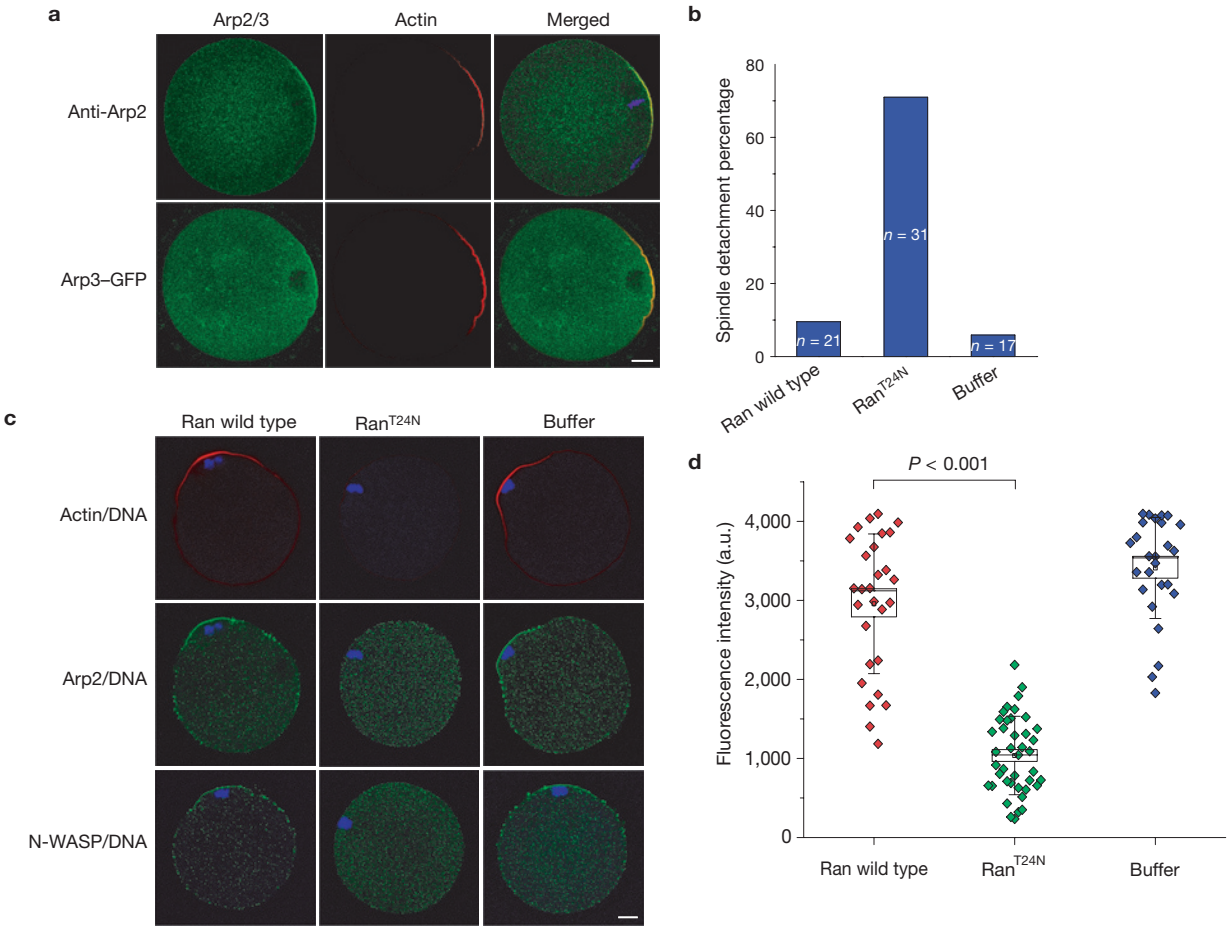

Figure 2 Ran signalling regulates cortical localization of the Arp2/3 complex. (**a**) Cortical cap localization of the Arp2/3 complex, as determined by anti-Arp2 immunostaining and Arp3–eGFP expression. In the anti-Arp2 panel, blue shows the DAPI (4,6-diamidino-2-phenylindole) staining of chromatin. Scale bar, 10 μm. (**b**) Quantification of spindle detachment percentage after Ran^{T24N} mutant protein microinjection. (**c**) Confocal micrographs showing Arp2 and N-WASP dislocalized in Ran^{T24N}-injected oocytes, but not in oocytes injected with wild-type Ran or buffer. In this experiment, nocodazole was used to prevent chromosome detachment from the cortex. Blue shows the DAPI staining of chromatin (DNA). Scale bar, 10 μm. (**d**) Quantification of cortical actin cap intensities stained with fluorescently labelled phalloidin in Ran-injected oocytes in the presence of nocodazole. $n = 28$ (Ran wild type), 41 (Ran^{T24N}) and 26 (buffer). The box range represents s.e.m.; whiskers show s.d.; the small square is the mean; and the line inside the box is the median.

these probes may have a preference for different populations of actin filaments.

We carried out high-resolution time-lapse confocal microscopy to observe the dynamics of the cytoplasmic actin network in oocytes expressing UtrCH–GFP. Kymograph analysis in the region near the cortical cap showed a retrograde flow of actin filaments from the cortical cap (Fig. 4a and Supplementary Movie S3). To quantitatively observe actin flow over the entire oocyte, we carried out spatiotemporal image correlation spectroscopy (STICS) analysis[27], which allows measurements of velocity vectors from spatial and temporal correlations of fluorescence intensity fluctuations from confocal image series. STICS analysis showed that the actin flow initiates with the highest velocity ($0.47 \pm 0.05\,\mu m\,min^{-1}$) from the cortical cap, down along both sides of the lateral cortex, and converges at the centre of the oocytes in the reverse direction towards the spindle (Fig. 4b). The high flow velocity near the cortical cap matches well with that estimated from the kymograph analysis ($0.59 \pm 0.09\,\mu m\,min^{-1}$). CK-666 treatment attenuates the high rate of actin flow from the cortical cap (Fig. 5a and see below).

The above observed actin flow is reminiscent of the actin retrograde flow at the leading edge of keratocytes or fibroblasts, which results from spatially separate actin polymerization and turnover[28]. To investigate the role of actin turnover, we incubated the oocyte with jasplakinolide, an actin-filament-stabilizing drug[29]. After 10 min incubation, the fine actin structures initiated from the cortical cap were replaced by much thicker actin bundles flowing towards the cell interior and accumulating at the spindle surface (Supplementary Fig. S5a and Movie S4). Indeed, cofilin, the highly conserved actin depolymerizing factor[30], was found to 'coat' the spindle, as detected by immunofluoresence staining using two different antibodies (Supplementary Fig. S3b). Jasplakinolide also caused nearly immediate cessation of actin flow in the oocyte interior (Supplementary Fig. S5b and Movie S4).

While imaging actin dynamics, we noticed coordinated movement of cytoplasmic particles under the differential interference contrast (DIC) channel. These particles exhibited streaming in a swirling pattern easily seen in a time-projected image (Fig. 4b and Supplementary Movies S5–S7). STICS analysis indicated that cytoplasmic particles streamed away from the cortical cap region

© 2011 Macmillan Publishers Limited. All rights reserved.

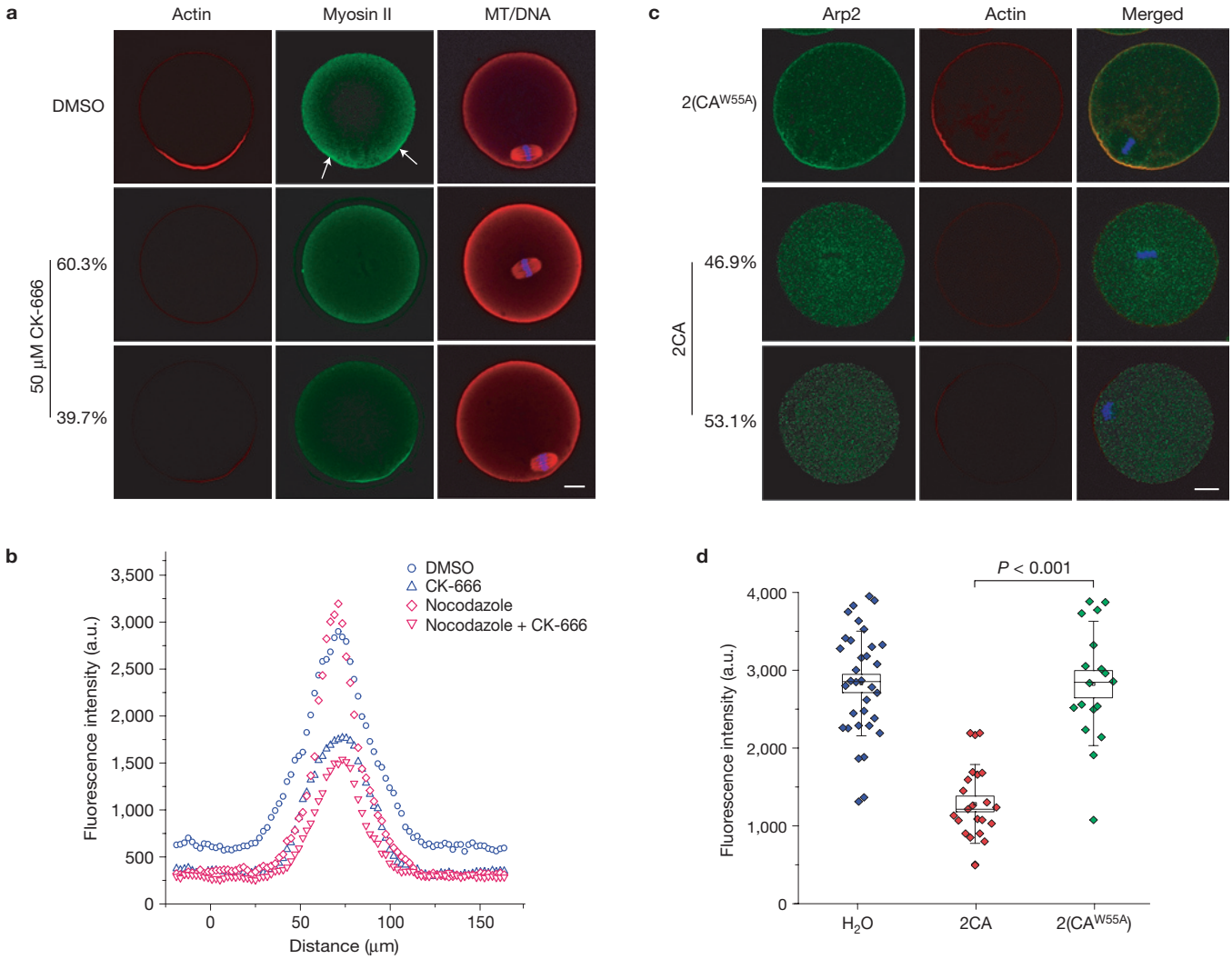

Figure 3 The Arp2/3 complex is required for most F-actin assembly in the cortical cap and for myosin-II ring maintenance. (**a**) Representative images showing actin and myosin-II localization by phalloidin staining and myosin-II immunostaining, respectively. All actin or myosin-II images were acquired in the same way so that their intensities can be compared across different conditions. The images were pseudo-coloured after data acquisition, and the images shown in the same row were from the same oocyte. Scale bar, 10 μm. Two classes of staining pattern, representing 60.3% and 39.7% of the total, were observed for CK-666-treated oocytes on the basis of spindle position. The myosin-II cortical ring appears as two intensity peaks flanking the actin cap (arrows, also see Supplementary Fig. S3a), whereas only a myosin-II cap was observed after CK-666 treatment. DNA, DAPI staining; MT, microtubule staining. (**b**) Quantification of cortical actin intensities in CK-666-treated and control oocytes (see Methods). The intensity trace of each group is the mean from 10 oocytes. (**c**) Peptide 2CA, but not 2(CA^{W55A}), disrupted the cortical localization of Arp2 and the actin cap. Two classes of staining pattern, representing 46.9% and 53.1% of the total, are shown for 2CA-injected oocytes on the basis of spindle position. Arp2 localization and the actin cap were disrupted even in oocytes with spindles remaining attached. Scale bar, 10 μm. (**d**) Quantification of cortical actin cap intensities in 2CA-, 2(CA^{W55A})- and H_2O-injected oocytes. $n = 34$ (H_2O), 22 (2CA) and 18 (2(CA^{W55A})). Box plots are as described in the caption of Fig. 2d.

along the cell periphery, arrived at the opposite pole of the oocyte and then circulated back in the central part of the oocyte towards the spindle (Fig. 4e). Observation of oocytes where the spindles were naturally oriented with their long axes at different angles relative to the confocal plane showed similar cytoplasmic streaming patterns (Fig. 4e and Supplementary Movies S5–S7), indicating that the streaming is rotationally symmetric around the axis through the spindle and cell centre. The cytoplasmic streaming was similar in pattern to that of the actin flow (compare Fig. 4b upper panel and Fig. 4e middle panel) and was eliminated completely by LatA or jasplakinolide (Supplementary Fig. S5b and Movie S4), indicating a dependence on dynamic actin assembly and disassembly.

We carried out a fluid dynamics simulation to evaluate whether the observed cytoplasmic streaming exerts a net force on the spindle to prevent its movement away from the cortex. The numerical simulation indicates that the cytoplasmic streaming is theoretically able to generate a net pressure on the spindle towards the cortex (Supplementary Fig. S6b,c). To experimentally observe this force, the spindle was disassembled by nocodazole treatment, and immediately afterwards the naked chromosomes were seen pushed towards the cortex at the same speed as cytoplasmic particles in the vicinity, until the chromatin was tightly abutting against the cortex (Fig. 4c). In a second experiment, we briefly treated oocytes with CK-666 (~20 min) such that the spindle began to move away from the cortex. We then transferred

© 2011 Macmillan Publishers Limited. All rights reserved.

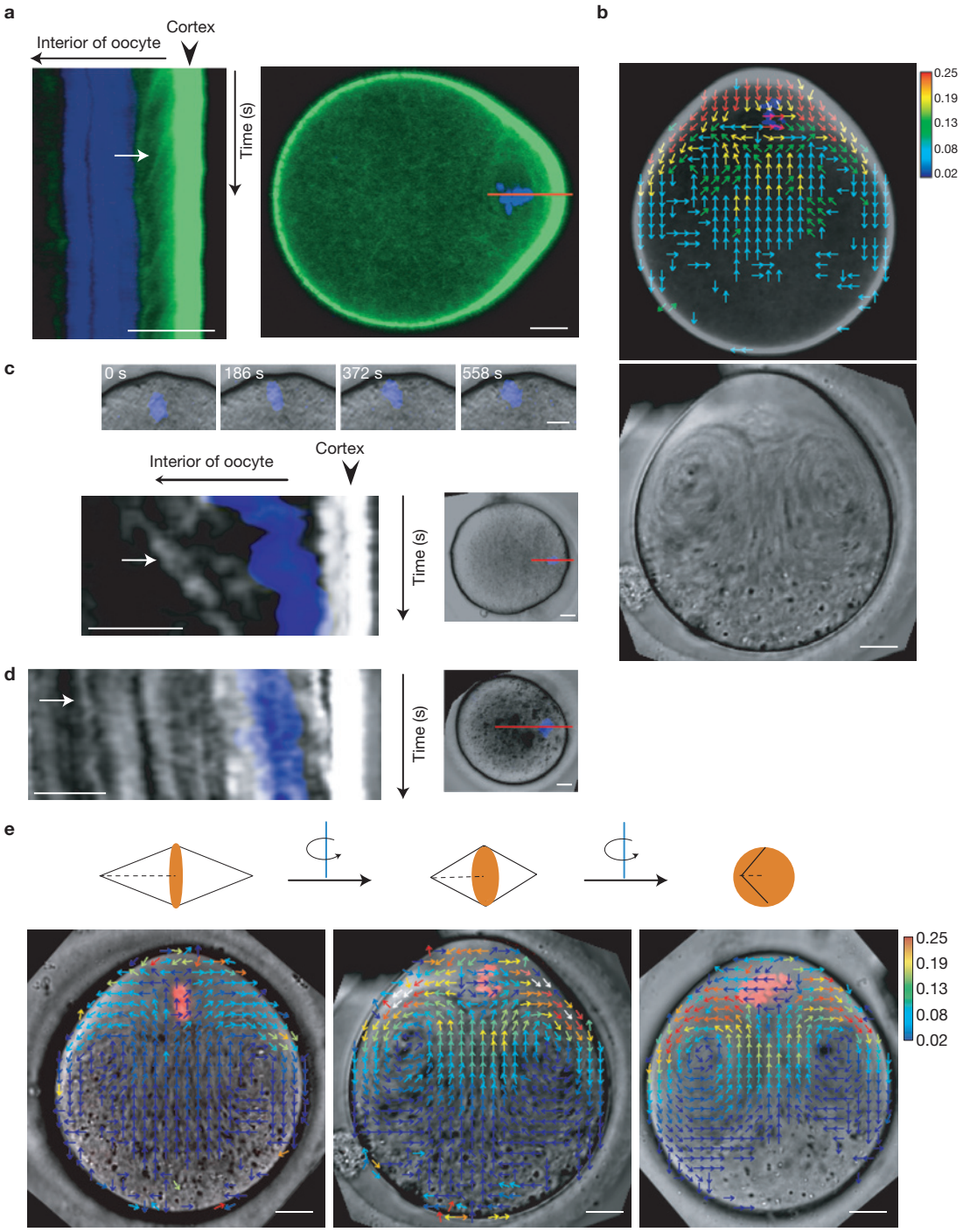

Figure 4 Cytoplasmic streaming powered by Arp2/3-complex-dependent actin flow generates a net pushing force on the spindle. (**a**) Kymograph (left), generated along the red line shown in the right panel, showing continuous F-actin flow (GFP fluorescence streaks from the cortex towards the oocyte interior, arrow pointing to one example) away from the cortical cap. Movie duration, 1,600 s. Scale bar, 10 μm. (**b**) Vector map of actin flow (from a UtrCH–GFP movie, top) in an MII oocyte obtained using STICS analysis. Heat bar unit, $\mu m\,min^{-1}$. The lower panel is a time projection of a DIC movie (Supplementary Movie S6) showing a swirling pattern of cytoplasmic particles. Scale bar, 10 μm. (**c**) Top, montage showing chromatin (blue) movement towards the cortex after spindle disassembly by nocodazole. Scale bar, 10 μm. Bottom, kymograph (left) along the red line in the right panel, of the same movie. For this kymograph and also for the one in **d**, to enhance the contrast of the transmitted light particles for the kymograph, an edge-detection (Sobel) filter was applied, resulting in white-coloured edges and cytoplasmic particles. Note the similar angle of the chromatin streak before arriving at the cortex to that of the streak by a cytoplasmic particle (white arrow), indicating that these entities were moving at similar rates. Movie duration, 2,670 s. Scale bars, 10 μm. (**d**) Kymograph (left), along the red line in the right panel, showing the spindle migrating back towards the cortex after drug wash-out in a CK-666-treated oocyte. Movie duration, 3,450 s. Note again, a cytoplasmic particle (white arrow) moving at the same speed as the chromatin. Scale bar, 10 μm. (**e**) Vector maps of cytoplasmic streaming generated by STICS in MII oocytes with different spindle orientations (as depicted in the illustration above each panel) relative to the confocal plane. Note the similar flow patterns in these different oocytes. Pink shows the Hoechst staining of chromatin. Scale bars, 10 μm.

© 2011 Macmillan Publishers Limited. All rights reserved.

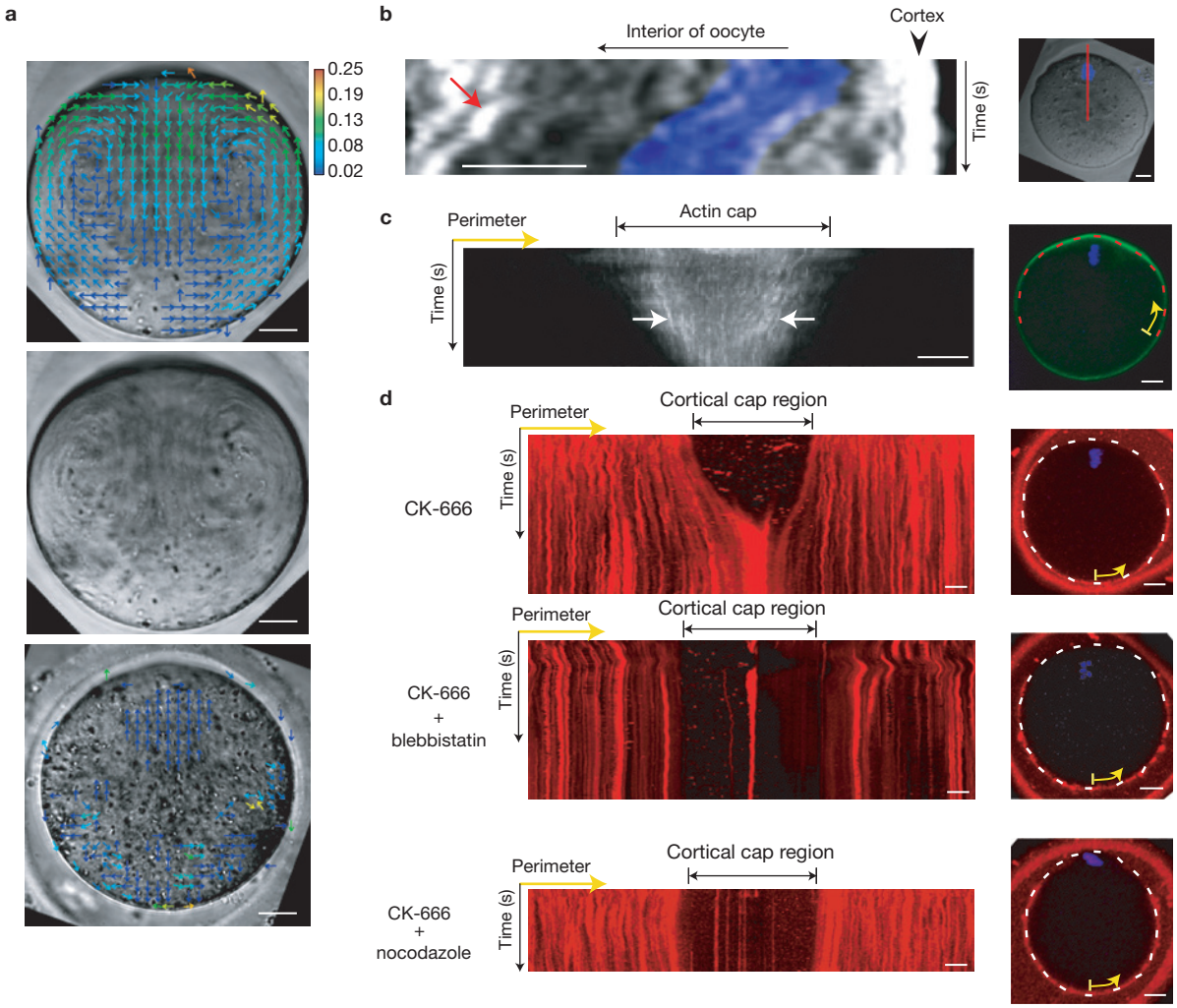

Figure 5 Myosin-II-dependent cortical cap contraction drives the MII spindle away from the cortex in the absence of Arp2/3 activity. (**a**) Vector maps of reverse cytoplasmic streaming in a CK-666-treated oocyte (top) and blocking of this reverse streaming by blebbistatin (bottom). Heat bar unit, $\mu m\,min^{-1}$. The middle panel is a time projection of the DIC movie of the same oocytes as in the top panel, showing a swirl pattern of cytoplasmic particles. Scale bar, 10 μm. (**b**) Kymograph (left) showing the spindle/chromatin (blue) movement away from the cortex at a rate similar to that of cytoplasmic particles (white streak, red arrow) after CK-666 addition. Movie duration, 2,070 s. The position of the line for kymograph generation is shown in the right panel. Scale bars, 10 μm. (**c**) Kymograph (left) generated along a line through the cortex of a UtrCH–GFP-expressing oocyte (dotted line, right panel), showing actin cap contraction after CK-666 addition. The yellow arrow in the right panel corresponds to the left edge of the kymograph. Movie duration, 2,245 s. Scale bars, 10 μm. Note the movement of actin structures (streaks, white arrows) from both sides towards the centre. (**d**) Kymograph (left) generated along a line through the cortex of a Texas-red–Con-A-labelled oocyte (dotted line, right panels, blue shows the Hoechst staining of chromatin) showing cortical cap contraction after CK-666 addition without (top) or with blebbistatin (middle), or with nocodazole (bottom). The yellow arrows in the right panels correspond to the left edges of the kymographs. The cap regions showed low-intensity ConA staining as marked. Movie durations, 4,395 s (top), 4,375 s (middle) and 2,035 s (bottom). Scale bars, 10 μm.

the oocytes to drug-free media. In oocytes where the spindle had not moved too far from the cortex, the actin-flow-powered cytoplasmic streaming resumed. Concomitantly, the spindle began to move back towards the cortex, with the particles behind moving at a similar speed (Fig. 4d). These experiments demonstrated that the actin-flow-driven cytoplasmic streaming exerts a force on the spindle towards the cortex.

Unexpectedly, CK-666 treatment not only disrupted the above cytoplasmic streaming but also activated a reverse streaming: particles now flowed towards the cortical cap along the sides of the oocyte and away from the spindle to the centre of the oocyte (Fig. 5a and Supplementary Movie S8). Importantly, this reverse cytoplasmic streaming after CK-666 addition is coupled with the spindle movement away from the cortex (Fig. 5b). Blebbistatin, which does not affect the normal actin flow and cytoplasmic streaming (Supplementary Movie S9), completely attenuated the reverse cytoplasmic streaming in the presence of CK-666 (Fig. 5a, bottom, Supplementary Movie S10), indicating that myosin-II contractility drives the reverse cytoplasmic streaming when Arp2/3 is inhibited. Simulation of the reverse streaming indicates that it can exert a force to cause the spindle to move away from the cortex (Supplementary Fig. S6d,e).

As myosin-II remained concentrated to the cortical cap in Arp2/3-inhibited oocytes (Fig. 3a), it was possible that the reverse cytoplasmic streaming was driven by contraction of the cortical cap. This was evident in oocytes expressing UtrCH–GFP treated with CK-666: the GFP cap rapidly decreased in size while the intensity near the cap centre remained constant (Fig. 5c and Supplementary Movie S11).

© 2011 Macmillan Publishers Limited. All rights reserved.

Another way to visualize cortical dynamics was by using fluorescent concanavalin A (ConA), which stains the cap region dimly relative to the rest of oocyte surface. Contraction of the ConA-dim zone can be readily observed after CK-666 addition and was blocked by blebbistatin (Fig. 5d and Supplementary Movies S12, S13). The myosin-II-driven cortical contraction in CK-666-treated oocytes was also inhibited by nocodazole (Fig. 5d and Supplementary Movie S14), explaining the suppression of spindle detachment by nocodazole after CK-666 treatment (Fig. 1a).

The results above demonstrate that MII chromosomes, through Ran signalling, localize and activate the Arp2/3 complex at the proximal cortex, and the Arp2/3 complex in turn functions to keep the chromosomes/spindle close to the cortex, maintaining MII oocyte polarity. The role of the Arp2/3 complex in maintaining spindle position is twofold. First, the Arp2/3 complex generates a continuous actin flow from the cortical cap, driving cytoplasmic streaming in a pattern leading to a net pressure on the spindle surface towards the cortical cap. Second, the Arp2/3 complex prevents myosin-II-driven contraction of the cortical cap, which generates a reverse cytoplasmic streaming possibly reminiscent of the myosin-II-driven fluid flow in fast-moving keratocytes[31]. Loss of asymmetric position of spindle/MII chromosomes is a known cause of impaired reproductive potential in ageing females[2,3,32]. As such, the spindle position is used as a clinical index to evaluate the quality of MII oocytes for *in-vitro* fertilization[33,34]. We speculate that the Arp2/3-regulated actin assembly may be necessitated by a requirement for a contraction-ready actomyosin cap, poising the oocytes to complete the second meiosis immediately on sperm entry. Maintaining spindle position under an active force may also prevent slow and random drift of spindle position or orientation if the meiotic arrest is prolonged. Finally, an active mechanism of spindle position maintenance that requires high energy expenditure (that is, to support constant actin polymerization and turnover), as opposed to a static mechanism, may impose a natural and stringent selection for oocytes possessing superior vitality to undergo zygotic development.□

METHODS

Methods and any associated references are available in the online version of the paper at http://www.nature.com/naturecellbiology

Note: Supplementary Information is available on the Nature Cell Biology website

ACKNOWLEDGEMENTS

We thank W. M. Bement (University of Wisconsin, USA) for providing pCS2+–UtrCH–GFP plasmid; J. Bamburg (Colorado State University, USA) for providing anti-cofilin and phos-cofilin antibodies; H. Cartwright (Stowers Institute, USA) for microfabricated wells for oocyte imaging; and M. Durnin and K. Westfahl (both Stowers Institute, USA) for technical assistance and mice maintenance. This work was supported in part by NIH grant P01 GM 066311.

AUTHOR CONTRIBUTIONS

K.Y. and R.L. designed the experiments, interpreted results and prepared the manuscript; K.Y. carried out all of the experiments; J.R.U. carried out STICS analysis with assistance from B.D.S. and also contributed to other image analysis; M.D. assisted in the initial experimental set-up. B.R. carried out the numerical simulations; R.L. conceived and supervised the project.

COMPETING FINANCIAL INTERESTS

The authors declare no competing financial interests.

Published online at http://www.nature.com/naturecellbiology
Reprints and permissions information is available online at http://www.nature.com/reprints

1. Sathananthan, A. H. Ultrastructure of the human egg. *Hum. Cell* **10,** 21–38 (1997).
2. Webb, M., Howlett, S. K. & Maro, B. Parthenogenesis and cytoskeletal organization in ageing mouse eggs. *J. Embryol. Exp. Morphol.* **95,** 131–145 (1986).
3. Kim, N. H., Moon, S. J., Prather, R. S. & Day, B. N. Cytoskeletal alteration in aged porcine oocytes and parthenogenesis. *Mol. Reprod. Dev.* **43,** 513–518 (1996).
4. Maro, B., Johnson, M. H., Webb, M. & Flach, G. Mechanism of polar body formation in the mouse oocyte: an interaction between the chromosomes, the cytoskeleton and the plasma membrane. *J. Embryol. Exp. Morphol.* **92,** 11–32 (1986).
5. Longo, F. J. & Chen, D. Y. Development of cortical polarity in mouse eggs: involvement of the meiotic apparatus. *Dev. Biol.* **107,** 382–394 (1985).
6. Verlhac, M. H., Lefebvre, C., Guillaud, P., Rassinier, P. & Maro, B. Asymmetric division in mouse oocytes: with or without Mos. *Curr. Biol.* **10,** 1303–1306 (2000).
7. Leader, B. *et al.* Formin-2, polyploidy, hypofertility and positioning of the meiotic spindle in mouse oocytes. *Nat. Cell Biol.* **4,** 921–928 (2002).
8. Deng, M., Suraneni, P., Schultz, R. M. & Li, R. The Ran GTPase mediates chromatin signaling to control cortical polarity during polar body extrusion in mouse oocytes. *Dev. Cell* **12,** 301–308 (2007).
9. Deng, M. & Li, R. Sperm chromatin-induced ectopic polar body extrusion in mouse eggs after ICSI and delayed egg activation. *PLoS One* **4,** e7171 (2009).
10. Brunet, S. & Maro, B. Cytoskeleton and cell cycle control during meiotic maturation of the mouse oocyte: integrating time and space. *Reproduction* **130,** 801–811 (2005).
11. Siller, K. H. & Doe, C. Q. Spindle orientation during asymmetric cell division. *Nat. Cell Biol.* **11,** 365–374 (2009).
12. Zhu, Z. Y. *et al.* Rotation of meiotic spindle is controlled by microfilaments in mouse oocytes. *Biol. Reprod.* **68,** 943–946 (2003).
13. Halet, G. & Carroll, J. Rac activity is polarized and regulates meiotic spindle stability and anchoring in mammalian oocytes. *Dev. Cell* **12,** 309–317 (2007).
14. Ayscough, K. R. *et al.* High rates of actin filament turnover in budding yeast and roles for actin in establishment and maintenance of cell polarity revealed using the actin inhibitor latrunculin-A. *J. Cell Biol.* **137,** 399–416 (1997).
15. Straight, A. F. *et al.* Dissecting temporal and spatial control of cytokinesis with a myosin II inhibitor. *Science* **299,** 1743–1747 (2003).
16. Nolen, B. J. *et al.* Characterization of two classes of small molecule inhibitors of Arp2/3 complex. *Nature* **460,** 1031–1034 (2009).
17. Goley, E. D. & Welch, M. D. The ARP2/3 complex: an actin nucleator comes of age. *Nat. Rev. Mol. Cell Biol.* **7,** 713–726 (2006).
18. Campellone, K. G. & Welch, M. D. A nucleator arms race: cellular control of actin assembly. *Nat. Rev. Mol. Cell Biol.* **11,** 237–251 (2010).
19. Padrick, S. B. *et al.* Hierarchical regulation of WASP/WAVE proteins. *Mol. Cell* **32,** 426–438 (2008).
20. Higgs, H. N., Blanchoin, L. & Pollard, T. D. Influence of the C terminus of Wiskott–Aldrich syndrome protein (WASp) and the Arp2/3 complex on actin polymerization. *Biochemistry* **38,** 15212–15222 (1999).
21. Wilde, A. *et al.* stimulates spindle assembly by altering microtubule dynamics and the balance of motor activities. *Nat. Cell Biol.* **3,** 221–227 (2001).
22. Li, H., Guo, F., Rubinstein, B. & Li, R. Actin-driven chromosomal motility leads to symmetry breaking in mammalian meiotic oocytes. *Nat. Cell Biol.* **10,** 1301–1308 (2008).
23. Schuh, M. & Ellenberg, J. A new model for asymmetric spindle positioning in mouse oocytes. *Curr. Biol.* **18,** 1986–1992 (2008).
24. Azoury, J. *et al.* Spindle positioning in mouse oocytes relies on a dynamic meshwork of actin filaments. *Curr. Biol.* **18,** 1514–1519 (2008).
25. Burkel, B. M., von Dassow, G. & Bement, W. M. Versatile fluorescent probes for actin filaments based on the actin-binding domain of utrophin. *Cell Motil. Cytoskeleton* **64,** 822–832 (2007).
26. Riedl, J. *et al.* Lifeact: a versatile marker to visualize F-actin. *Nat. Methods* **5,** 605–607 (2008).
27. Hebert, B., Costantino, S. & Wiseman, P. W. Spatiotemporal image correlation spectroscopy (STICS) theory, verification, and application to protein velocity mapping in living CHO cells. *Biophys. J.* **88,** 3601–3614 (2005).
28. Cramer, L. P. Molecular mechanism of actin-dependent retrograde flow in lamellipodia of motile cells. *Front. Biosci.* **2,** d260–d270 (1997).
29. Bubb, M. R., Senderowicz, A. M., Sausville, E. A., Duncan, K. L. & Korn, E. D. Jasplakinolide, a cytotoxic natural product, induces actin polymerization and competitively inhibits the binding of phalloidin to F-actin. *J. Biol. Chem.* **269,** 14869–14871 (1994).
30. Chen, H., Bernstein, B. W. & Bamburg, J. R. Regulating actin-filament dynamics *in vivo*. *Trends Biochem. Sci.* **25,** 19–23 (2000).
31. Keren, K., Yam, P. T., Kinkhabwala, A., Mogilner, A. & Theriot, J. A. Intracellular fluid flow in rapidly moving cells. *Nat. Cell Biol.* **11,** 1219–1224 (2009).
32. Miao, Y. L., Kikuchi, K., Sun, Q. Y. & Schatten, H. Oocyte aging: cellular and molecular changes, developmental potential and reversal possibility. *Hum. Reprod. Update* **15,** 573–585 (2009).
33. Cohen, Y. *et al.* Spindle imaging: a new marker for optimal timing of ICSI? *Hum. Reprod.* **19,** 649–654 (2004).
34. Moon, J. H. *et al.* Visualization of the metaphase II meiotic spindle in living human oocytes using the Polscope enables the prediction of embryonic developmental competence after ICSI. *Hum. Reprod.* **18,** 817–820 (2003).

© 2011 Macmillan Publishers Limited. All rights reserved.

METHODS

Mouse oocyte collection and culture. All animals used in this research were handled in accordance with guidelines defined by the Institutional Animal Care and Use Committee (IACUC) of Stowers Institute. Mouse MII oocytes were collected from 5- to 9-week-old CD1 mice and cultured in M16 medium (Chemicon) at 37 °C in a 5% CO_2 atmosphere. For drug treatment experiments, the medium was supplemented with 50 μM or 100 μM CK-666 (Chemdiv) as indicated in the text, 10 μM nocodazole (Sigma), 50 μM LatA (Invitrogen) and/or 100 μM blebbistatin (EMD Biochemicals). A corresponding amount of dimethylsulphoxide (DMSO; the solvent of the chemicals) was used in control groups. For live-cell imaging, the oocytes were cultured in a MatTek glass-bottom Petri dish (MatTek) in a custom chamber maintained at 37 °C under a 5% CO_2 atmosphere.

Plasmid construction, *in vitro* synthesis of mRNA, and morpholino. Arp3–eGFP (from M. Welch, UC Berkeley, USA, Addgene #8462), 2CA and 2(CA^{W55A}) were inserted into pRL and pRL–eGFP respectively, both of which were derived from pT7TS (from P. Krieg, The University of Arizona, USA, Addgene #17901). The F-actin probe pCS2+–UtrCH-eGFP was a gift from W. Bement. Capped mRNA was synthesized from a linearized plasmid template using T7 or SP6 mMessage mMachine (Ambion), poly-A tailed with Poly(A) Tailing kit, and then purified with MEGAclear kit (Ambion). Morpholino stock solution was prepared with H_2O as suggested by the manufacturer (Gene Tools), and a needle concentration of 0.2 mM was applied for microinjection. A standard control morpholino oligonucleotide was injected as a control. The sequence of the morpholino oligonucleotide used for N-WASP knockdown is 5′-TGGAGCGTCCAGGGTCGTCACTTCT-3′.

Antibodies and immunostaining. After removal of the zona pellucida with Tyrode's acidic solution, the oocytes were fixed in 3.75% paraformaldehyde in PBS and blocked with 0.1 M glycine solution. Antibody incubation was carried out at 4 °C overnight after permeabilizing with 0.1% Triton X-100 for 15 min and blocking with 0.3% BSA and 0.01% Tween 20 in PBS. The primary antibodies used were: rabbit anti-Arp2 (Santa Cruz, 1:200), mouse anti-α-tubulin (Sigma, 1:2,000), rabbit anti-non-muscle myosin-II heavy chain A and B (Covance, 1:1,000) and rabbit anti-N-WASP (Santa Cruz, 1:300). The oocytes were then stained with Alexa-488-labelled and/or Alexa-546-labelled anti-mouse or anti-rabbit secondary antibody (Molecular Probes, 1:300). Image acquisition of fixed oocytes was carried out using a ×40 objective on a Zeiss LSM510 (Jena) confocal microscope.

Microinjection and time-lapse confocal microscopy. Microinjection was carried out in M2 medium (Chemicon) using Narishige micromanipulators. Typically, 10 to 12 pl (approximately 4% of the oocyte volume) of 1–2 μg μl^{-1} mRNA was injected into the oocytes. Injection of Ran^{T24N} was conducted with a needle concentration of 129.04 μM, which gave rise to a final concentration of approximately 5.16 μM in injected oocytes. Time-lapse imaging was carried out with an LSM 510 META microscope (Carl Zeiss) equipped with a Plan Apochromat ×40/1.2 NA water-immersion objective. UtrCH–eGFP was excited with a 488 nm argon laser and detected with a 505–550 nm band-pass filter. Only oocytes that expressed a moderate level of UtrCH–eGFP were chosen for imaging and further analysis, because excessive expression of the probe interfered with spindle detachment on Arp2/3 inactivation. Hoechst 33342 (10 ng ml^{-1}) was included in the culture medium for chromatin staining as an indicator of spindle position. To detect cortical cap contraction, oocytes were labelled with 40 μg ml^{-1} Texas-red-labelled ConA for 30 min before imaging.

Statistical analysis. Statistical analysis of the data was carried out in Excel and/or Origin Lab Pro. *P* values were determined using Student's *t*-test.

STICS analysis and velocity field measurement. Velocity fields for transmitted light and fluorescence were obtained using the STICS method similar to related particle image velocimetry and 'speckle' methods[27,35,36]. The spatiotemporal correlation methods have been used for a wide variety of transmitted and reflected light applications including granular particles[37,38], embryonic cell migration[35] and blood cell flow[39,40]. Images were preprocessed first by alignment. In situations where oocyte rotation was observed, alignment of transmitted light images and actin images was carried out using the StackReg plugin written for ImageJ. In situations where Hoechst co-registration was important, alignment was carried out by centroid tracking of the masked transmitted light image. The mask was created using either direct thresholding or thresholding of the edge-enhanced (Sobel) image followed by binary fill operations and area- or position-based removal of thresholded regions not corresponding to the oocyte. After alignment, stationary structures were removed from the images by subtraction of the time-averaged image from each frame. The average intensity for each image before subtraction was added back uniformly to each subtracted image to prevent negative intensities. Finally, a region of interest was generated excluding the oocyte cortex, taking care to avoid momentary fluctuations of the cortex. The area outside this region was uniformly filled with the average intensity inside the region. Spatiotemporal correlation was then carried out in 32 × 32 pixel regions with a 16 pixel overlap between the regions to allow for highly localized motions to be accurately represented using the fast Fourier transform method[27]. The average particle displacement within the correlation image is represented by the maximum of the spatial cross-correlation between two images separated in time. Maxima were found by smoothing the correlation image and then fitting the nine pixels surrounding the maximum pixel to a simple polynomial ($f(x,y) = ax^2 + bx + c + dy^2 + ey$). The maximum is then given by $(-b/2a, -e/2d)$. The time correlation shift was three frames for transmitted light and one frame for actin. All velocities were converted to micrometres per minute and represented by arrows centred on each analysis region with normalized lengths and colours corresponding to the velocity magnitude. This method was implemented with custom plugins written in Java for ImageJ, available for download at (http://research.stowers.org/imagejplugins).

For particle-tracking measurements, first large features were removed from the movie using the ImageJ rolling-ball background-subtraction method with a ball radius of three pixels. Then particle tracking was carried out using the MOSAIC ParticleTracker plugin for ImageJ[41] with a particle radius of three pixels, a pixel-detection percentage of 0.2%, a linking range of two frames and a maximum displacement between frames of ten pixels. The trajectories were then averaged into regions similar to those measured with STICS for comparison. These measurements are noisy and limited by the contrast and persistence of the transmitted light particles but did show similar flow patterns and velocities to the STICS measurements (Supplementary Fig. S5c). The fluorescence STICS measurements were validated by manual measurement of the most prominent lines observed in the wild-type UtrCH–GFP kymograph (Fig. 4a). Analysis of slopes for the seven brightest lines gave an average velocity of 0.59 ± 0.09 μm min^{-1}, close to the average velocity of 0.47 ± 0.05 μm min^{-1} measured with STICS analysis of thresholded movies to exclude dim particles.

Kymograph generation. Before kymograph generation, images were aligned as discussed above for the velocity field analysis. Additional kymograph alignment was carried out in situations where large cortical displacement was observed by aligning to the edge of the transmitted light cortex for each line in the kymograph. Kymographs of chromatin detachment were obtained by first carrying out an edge-finding filter (Sobel) on the smoothed transmitted light image for enhanced visualization of transmitted light particles with poor contrast. Kymographs were typically averaged over a width of five pixels to portray representative behaviour.

Membrane profile kymographs of ConA and cortical actin cap contraction were obtained by first segmenting out the cortex. In the case of actin, the actin signal itself is strongly cortical and a smoothed image with a rolling-ball background subtraction can be thresholded to yield a cortical mask. The mask was then dilated as needed to ensure complete cortex coverage. For ConA, the large number of aggregates outside the cortex made it difficult to segment the membrane. We hence inverted the image and smoothed it before segmenting out the cytosol, filling holes to prevent voids in the cytosol. This mask was then dilated so that it encompassed the membrane and then an XOR (ImageJ) operation was carried out with the original mask to create a membrane mask. Once the membrane masks were generated, 360 line profiles were generated from the centre of the oocyte, allowing non-zero values only in the cortical masked regions. The maxima of these profiles were plotted as a function of angle and time to obtain the kymograph.

Numerical simulation of fluid dynamics in mouse oocyte. The fluid flow was simulated by numerical solution of the Navier–Stokes equation for the incompressible fluid $\partial\mathbf{u}/\partial t + \mathbf{u}\cdot\nabla\mathbf{u} = -(1/\rho)\nabla p + \nu\nabla^2\mathbf{u}$, where $\mathbf{u}$ denotes the fluid velocity, p is the pressure and ρ and ν are the density and kinematic viscosity of the fluid, respectively[42]. This equation describes the two-dimensional (2D) flow velocity field as well as the distribution of the fluid pressure in the circular region with an obstacle permanently fixed at a specified location representing an immovable spindle. Simplification of the 3D system to a 2D representation is justified by the observed rotational symmetry in the fluid flow pattern (Fig. 4e and main text). The no-slip (zero velocity) boundary conditions were imposed on the circular boundary. In untreated oocytes, we assumed a flow source placed above the spindle obstacle at the midpoint between the obstacle and the upper circular boundary at the symmetry axis of the system. In CK-666-treated oocytes, the actomyosin contraction was mimicked by placing a sink in the same location as described above. We considered the spindle

© 2011 Macmillan Publishers Limited. All rights reserved.

DOI: 10.1038/ncb2320

as a solid impenetrable obstacle, where the no-slip boundary conditions were imposed, and also as a partially penetrable obstacle by replacing the solid structure with a region with a viscosity three times higher than that outside this region. The simulations were carried out with COMSOL Multiphysics 3.4 finite-element method software using the finest possible non-uniform adaptive mesh.

35. Zamir, E. A., Czirok, A., Rongish, B. J. & Little, C. D. A digital image-based method for computational tissue fate mapping during early avian morphogenesis. *Ann. Biomed. Eng.* **33,** 854–865 (2005).
36. Ponti, A., Vallotton, P., Salmon, W. C., Waterman-Storer, C. M. & Danuser, G. Computational analysis of F-actin turnover in cortical actin meshworks using fluorescent speckle microscopy. *Biophys. J.* **84,** 3336–3352 (2003).
37. Pudasaini, S. P., Hsiau, S-S., Wang, Y. & Hutter, K. Velocity measurements in dry granular avalanches using particle image velocimetry technique and comparison with theoretical predictions. *Phys. Fluids* **17,** 093301 (2005).
38. Lueptow, R. M., Akonur, A. & Shinbrot, T. PIV for granular flows. *Exp. Fluids* 183–186 (1998).
39. Rossow, M., Mantulin, W. W. & Gratton, E. Spatiotemporal image correlation spectroscopy measurements of flow demonstrated in microfluidic channels. *J. Biomed. Opt.* **14,** 024014 (2009).
40. Rossow, M. J., Mantulin, W. W. & Gratton, E. Scanning laser image correlation for measurement of flow. *J. Biomed. Opt.* **15,** 026003 (2010).
41. Sbalzarini, I. F. & Koumoutsakos, P. Feature point tracking and trajectory analysis for video imaging in cell biology. *J. Struct. Biol.* **151,** 182–195 (2005).
42. Landau, L. D. & Lifshitz, E. M. *Course of Theoretical Physics* Vol. 6 (Pergamon, 1987).

© 2011 Macmillan Publishers Limited. All rights reserved.

nature cell biology

DOI: 10.1038/ncb2320

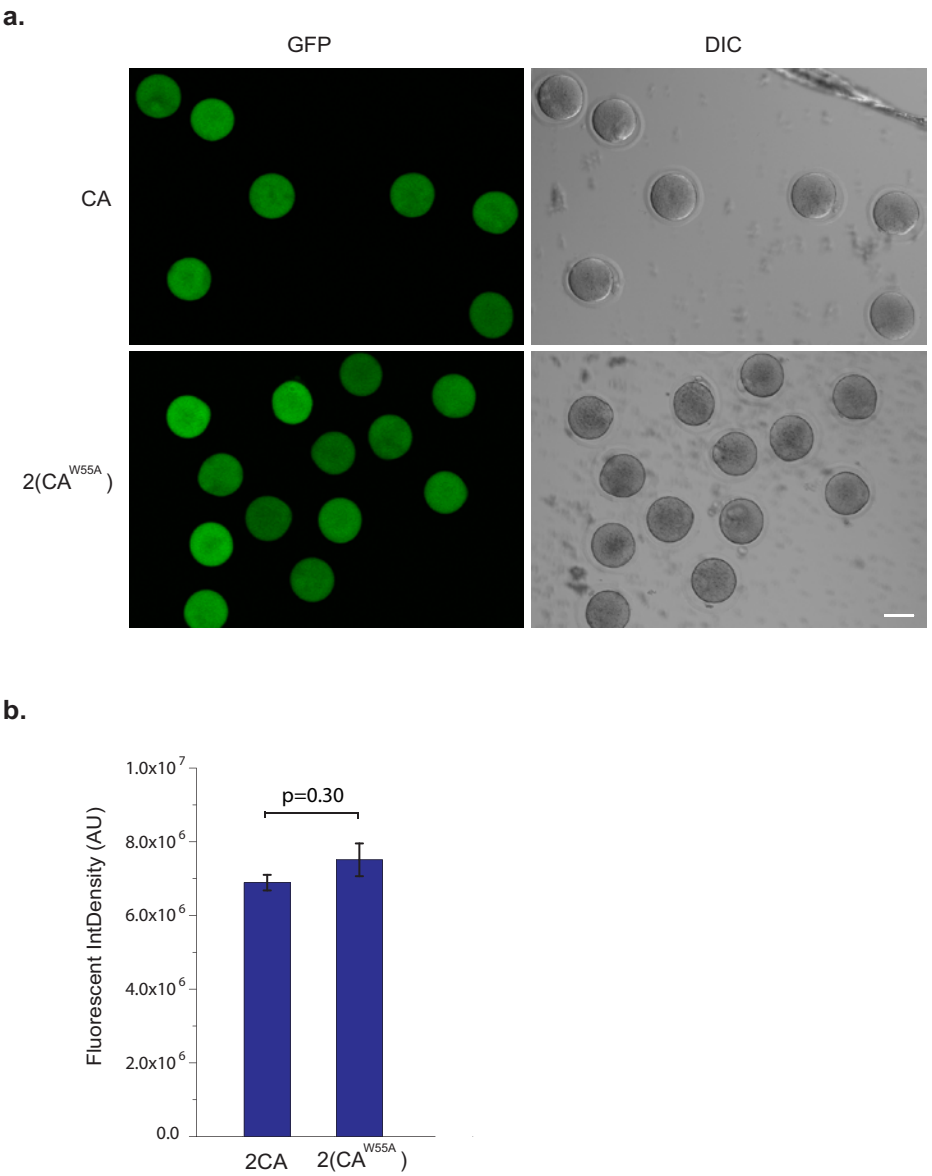

Figure S1 Constructs 2CA and 2(CA^{W55A}) were expressed at similar levels in mouse oocytes. (a) Representative images of mouse oocytes expressing GFP-tagged inhibitory peptide 2CA and its mutant 2(CA^{W55A}). Scale bar: 50 μm. (b) Quantification of GFP fluorescent integrative intensities of 2CA and 2(CA^{W55A})-expressing oocytes. Shown are mean±s.e.m (30 oocytes analyzed).

© 2011 Macmillan Publishers Limited. All rights reserved.

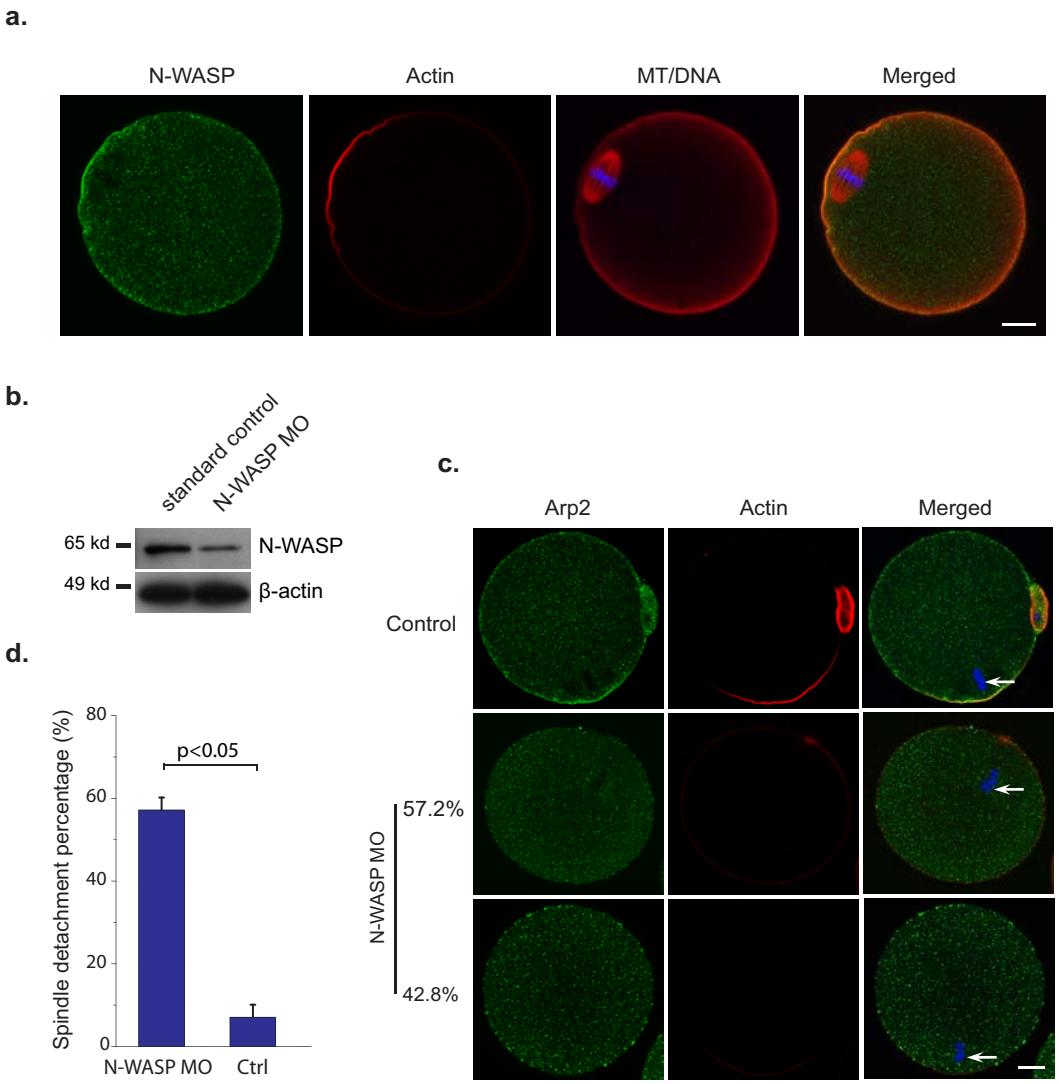

Figure S2 N-WASP knockdown disrupts cortical localization of Arp2/3 complex, and induces spindle detachment from the cortex. (a) Similar to Arp2/3 complex, N-WASP is localized to the cortical cap in mouse MII oocyte. Scale bar: 10 μm. (b) Morpholino microinjection down-regulates the N-WASP level in MII oocytes. N-WASP level decreased significantly in N-WASP MO injected oocytes, as compared with standard control morpholino injected oocytes (approximately 40 oocytes were used for the sample in each lane). (c) Confocal images showing Arp2 dislocalized in N-WASP MO-injected oocytes, but not in standard control morpholino injected oocytes. Notice that two classes of staining patterns, representing 57.2% and 42.8% of total, are shown for N-WASP MO injected oocytes based on spindle position. Arp2 is dislocalized even in oocytes with spindles still located in the subcortex, indicating it is not because of the lack of chromatin signal. Blue shows the DAPI staining of chromatin (arrows). Scale bar: 10 μm. (d) Quantification of spindle detachment percentage after N-WASP knockdown by morpholino microinjection. Data are mean±s.e.m (4 experiments, 89 oocytes analyzed).

© 2011 Macmillan Publishers Limited. All rights reserved.

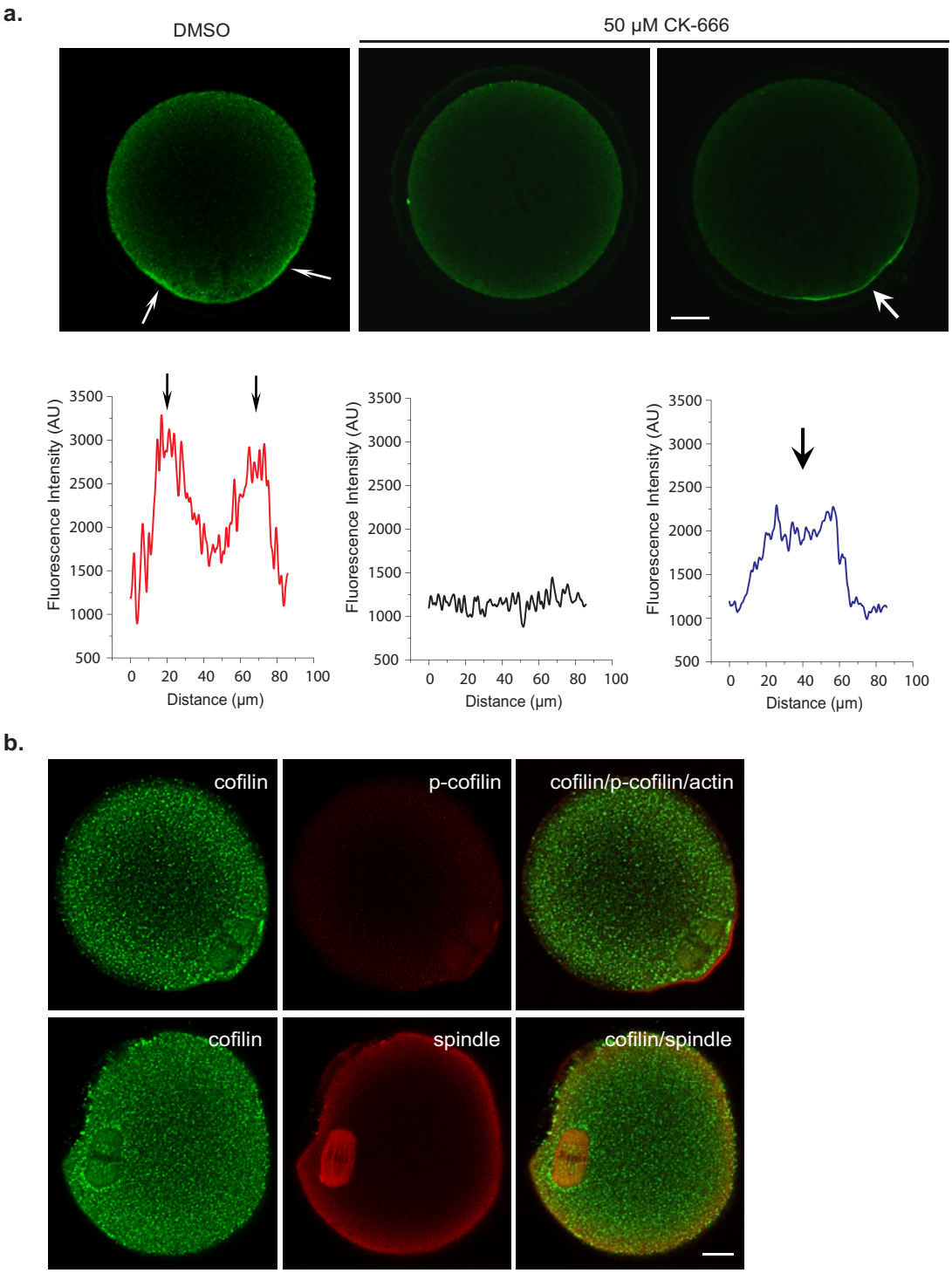

Figure S3 (a) Fluorescence quantification profile of myosin II intensity in the cortical cap region. The cortical myosin II fluorescent intensity of oocytes shown in Fig3a is quantified with line-scan analysis (lower panels). In DMSO treated control oocyte, myosin II organizes into a ring, shown as two fluorescent peaks (black arrows, corresponding to the two white arrows in the image) in the shown cross section (confocal plane) of the oocyte, whereas in CK-666 treated oocytes, myosin II either reorganizes into a cap shown as one broad peak (black arrow; when chromatin was still in vicinity), or dissociated from cortex (when chromatin was detached from cortex). White arrow indicates the fluorescent peaks in the confocal image. Scale bar: 10 μm. (b) Cofilin concentrates at the surface of the MII spindle. MII oocytes were fixed and stained with mouse anti-cofilin (upper left panel, antibody provided by Bamburg lab), rabbit anti-phos-cofilin (upper middle panel, antibody provided by Bamburg lab) and rabbit anti-cofilin (lower left panel, antibody purchased from Cell Signaling). In the merged image (top right), actin was also stained in red with phalloidin. Scale bar: 10 μm.

© 2011 Macmillan Publishers Limited. All rights reserved.

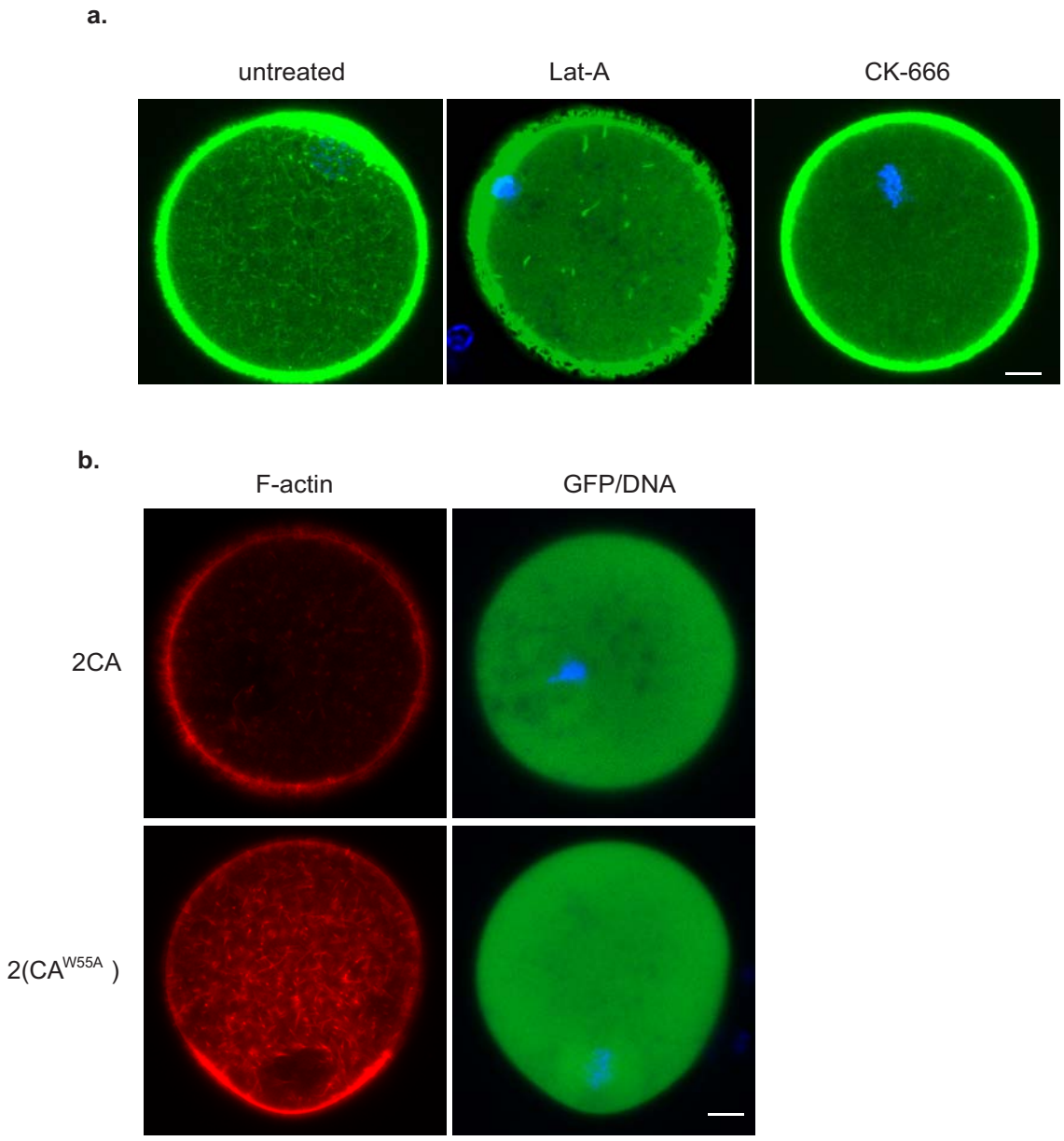

Figure S4 Cytoplasmic F-actin network is grossly disrupted by inhibiting Arp2/3 activity. (a) Representative images showing F-actin network in untreated oocyte, or oocyte treated with LatA, or CK-666. LatA disrupted the fine actin network in oocyte cytoplasm, however, a few F-actin structures remained and formed thick actin bars. In CK-666 treated oocyte, the density of the fine actin network was dramatically reduced. Scale bar: 10 μm. (b) Representative images showing cytoplasmic F-actin network in 2CA and 2(CA^{W55A}) expressing oocytes. To observe the cytoplasmic F-actin network, mouse oocytes expressing GFP-tagged 2CA or 2(CA^{W55A}) were microinjected with rhodamine phalloidin to label F-actin. 2CA disrupted the fine actin network in oocyte cytoplasm, whereas W55A mutation abolished this effect. GFP channel shows the expression of 2CA or 2(CA^{W55A}), and blue shows the Hoechst staining of chromatin. Scale bar: 10 μm.

© 2011 Macmillan Publishers Limited. All rights reserved.

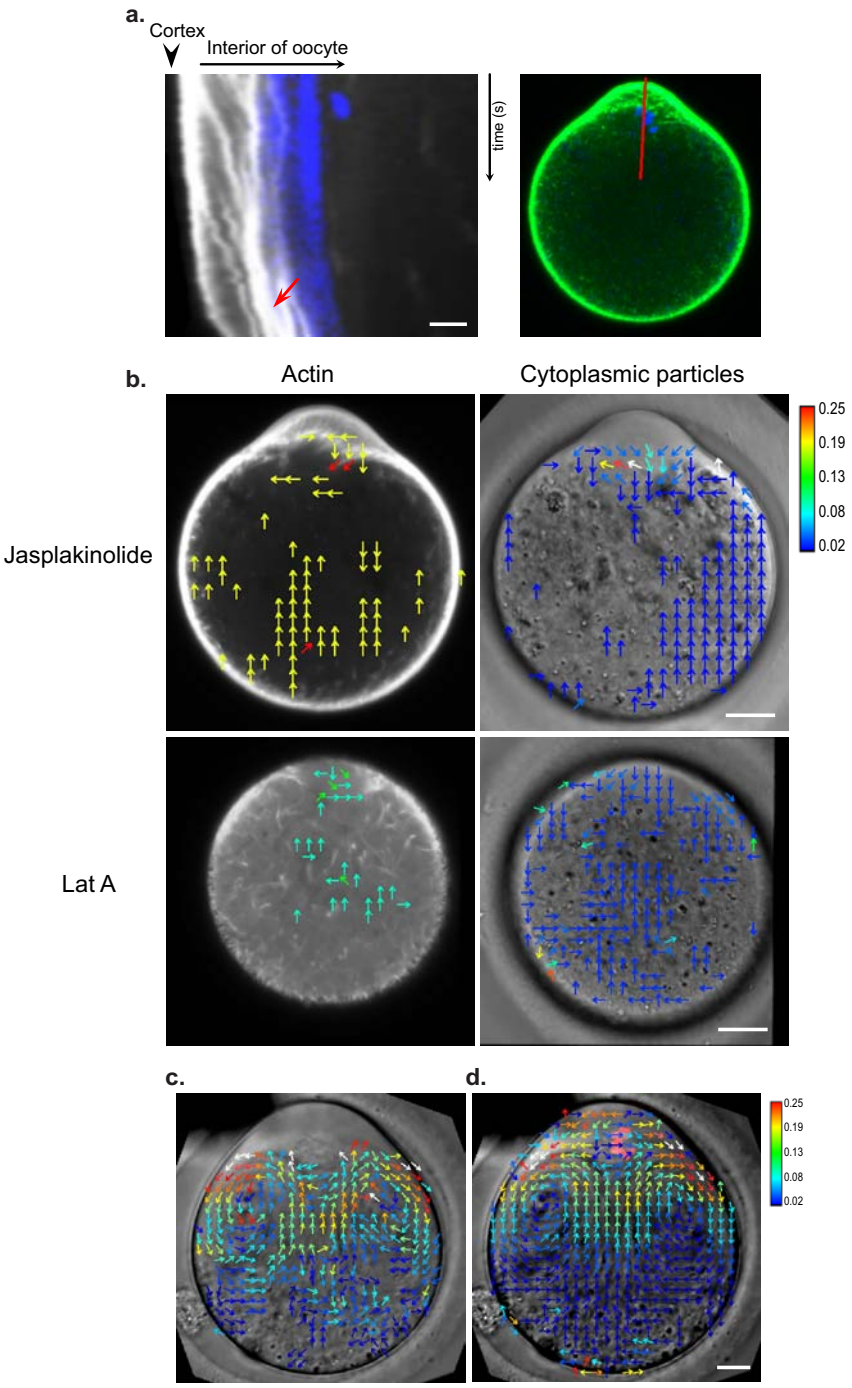

Figure S5 Actin stabilizer (jasplakinolide) and inhibitor (LatA) blocked cytoplasmic streaming in MII oocytes. (a) Kymograph analysis of F-actin dynamics in 500 nM jasplakinolide treated oocyte. Thick actin streaks (left of chromatin, red arrow) accumulated at the surface of the spindle. Movie duration: 2070 s. The right panel shows a still image and indicates the line along which the kymograph was generated. Scale bar: 5 μm. (b) Jasplakinolide or LatA-treatment abolished actin flow and cytoplasmic streaming. Vector map of actin dynamics (left) and cytoplasmic particles (right) in MII oocyte treated with jasplakinolide or LatA, as determined by STICS analysis. Heat bar unit: μm/min. The vector maps show minimal motions. Scale bar: 10 μm. (c) Particle tracking measurement of cytoplasmic streaming in MII oocyte. Flow map creating from averaged tracked particle motions (see supplementary Methods) over the same regions as our STICS analysis, showing a similar flow velocity pattern and magnitude to the STICS analysis (d). Notice particle tracking was unable to report any flow information in the subcortical region above the spindle due to the paucity of transmitted light particles in this region. Scale bar: 10 μm.

© 2011 Macmillan Publishers Limited. All rights reserved.

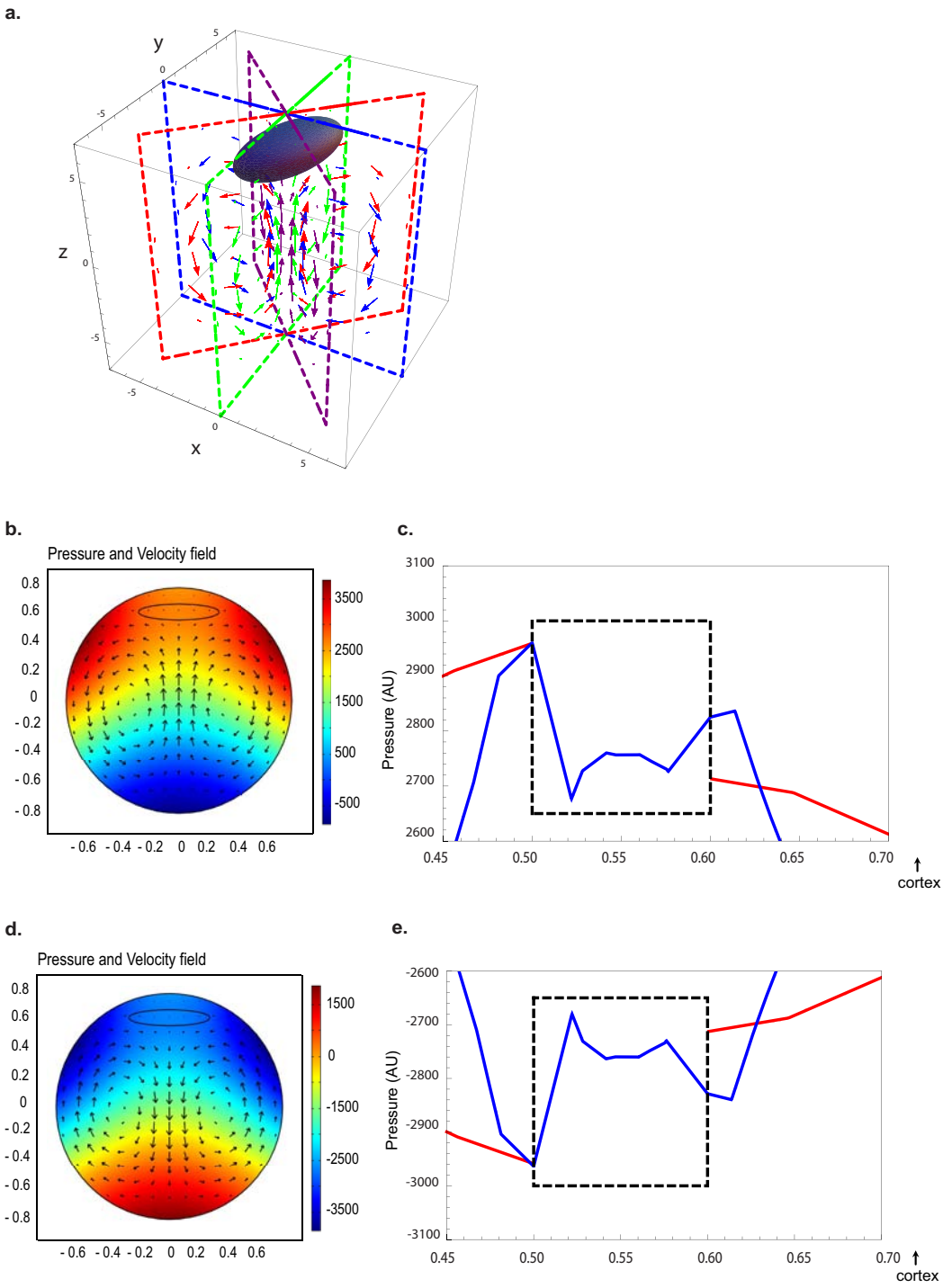

Figure S6 Numerical simulation of fluid dynamics in mouse oocyte. (a) A schematic diagram showing that the observed cytoplasmic streaming in mouse oocyte is rotationally symmetric around the axis drawn through spindle and the center of the cell, based on the vector maps in different confocal planes presented in Figure 4e. Although our data does not rule out streaming in planes perpendicular to the above axis, such streaming is not expected to exert pressure on the spindle. (b) Pressure and velocity field maps from fluid dynamics simulation of untreated MII oocytes with the source of flow above the spindle and below the cortical cap. (c) A plot of fluid pressure from the simulation in (b) as a function of the position along the axis through the spindle and cortical cap centers (y axis). Red curve represents the case of spindle considered as a solid impenetrable obstacle, whereas the blue one corresponds to the case where spindle is considered partially penetrable modeled as a region with higher viscosity. The dashed rectangle represents the spindle region. Notice the higher pressure at the spindle surface away from the cortical cap than that at the side facing the cortex. (d) Pressure and velocity fields simulated for CK-666-treated oocytes having a reverse cytoplasmic streaming due to cortical cap contraction. (e) A plot of fluid pressure from the simulation in (d) as a function of the position along the axis through spindle and cortical cap centers (y). Notice the higher pressure at the spindle surface facing the cortical cap than that away from the cortex.

© 2011 Macmillan Publishers Limited. All rights reserved.

Blots from Fig S2b

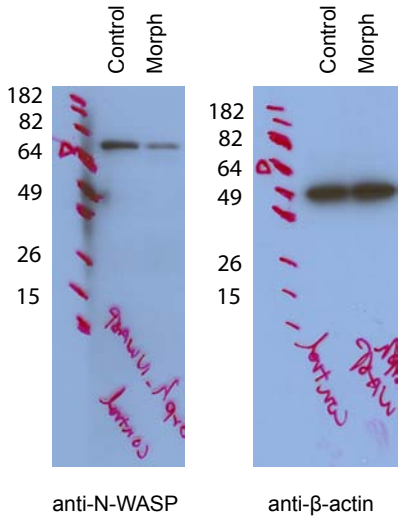

Figure S7 Full scans

© 2011 Macmillan Publishers Limited. All rights reserved.

Supplementary Movie Legends

Supplementary Movie 1 Inhibition of Arp2/3 activity caused spindle to detach from the cortex. Time-lapse imaging of a MII oocyte treated with CK-666. Blue shows the Hoechst staining of chromatin. Frames are 93 s apart and movie length is 2246 s.

Supplementary Movie 2 Blebbistatin prevents spindle detachment from the cortex due to CK-666 treatment. Time-lapse imaging of a MII oocyte treated with CK-666 and blebbistatin. Blue shows the Hoechst staining of chromatin. Frames are 60 s apart and movie length is 2340 s.

Supplementary Movie 3 Arp2/3-dependent actin flow and cytoplasmic streaming in MII oocyte. Time-lapse imaging of a MII oocyte expressing F-actin probe UtrCH-GFP. Notice the distinct F-actin structures flowing away from the cortical cap. Frames are 10 s apart and movie length is 1600 s.

Supplementary Movie 4 Jasplakinolide blocks cytoplasmic streaming in MII oocyte. Time-lapse imaging of a MII oocyte expressing F-actin probe UtrCH-GFP treated with 500 nM jasplakinolide. Frames are 16 s apart and movie length is 2070 s.

Supplementary Movie 5 Time-lapse imaging of a MII oocyte showing cytoplasmic streaming in MII oocyte. The same oocyte was used for STICS analysis in Fig. 4e, left panel. Blue shows the Hoechst staining of chromatin. Frames are 136 s apart and movie length is 3944 s.

Supplementary Movie 6 Time-lapse imaging of a MII oocyte showing cytoplasmic streaming in MII oocyte. The same oocyte was used for STICS analysis in Fig. 4e, middle panel. Blue shows the Hoechst staining of chromatin. Frames are 136 s apart and movie length is 4080 s.

Supplementary Movie 7 Time-lapse imaging of a MII oocyte showing cytoplasmic streaming MII oocyte. The same oocyte was used for STICS analysis in Fig. 4e, right panel. In this oocyte, the F-actin was also labeled with UtrCH-GFP. Blue shows the Hoechst staining of chromatin. Frames are 126 s apart and movie length is 5796 s.

Supplementary Movie 8 Reverse cytoplasmic streaming in MII oocyte when Arp2/3 activity is inhibited. Time-lapse imaging of a MII oocyte treated with CK-666. Under this condition, the cytoplasmic streaming occurs in a reverse direction from that shown in Movie S5, 6 and 7. Frames are 125.5 s apart and movie length is 5287 s.

Supplementary Movie 9 Blebbistatin has no effect on actin flow or cytoplasmic streaming in the absence of CK-666. Time-lapse imaging of a MII oocyte treated with blebbistatin, showing normal actin flow and cytoplasmic streaming after inhibition of Myosin II activity. Frames are 125.5 s apart and movie length is 5773 s.

Supplementary Movie 10 Blebbistatin completely abolishes the reverse cytoplasmic streaming after Arp2/3 inhibition. Time-lapse imaging of a MII oocyte treated with CK-666 and blebbistatin, showing the attenuation of reverse cytoplasmic streaming after inhibition of Myosin II activity. Frames are 125.5 s apart and movie length is 5287 s.

Supplementary Movie 11 Actin cap contraction in MII oocyte after CK-666 addition. Time-lapse imaging of a MII oocyte expressing UtrCH-GFP treated with CK-666. The power of Argon laser was adjusted to allow imaging of the cortical actin cap. Notice that the actin cap rapidly reduces in size while the intensity near the cap center remains constant. Frames are 10 s apart and movie length is 2130 s.

Supplementary Movie 12 Cortical cap contraction in oocyte stained with Texas Red labeled ConA. Time-lapse imaging of a ConA-stained oocyte treated with CK-666. Blue shows the Hoechst staining of chromatin. Frames are 34.5 s apart and movie length is 3760 s.

Supplementary Movie 13 Blebbistatin inhibits cortical cap contraction. Time-lapse imaging of a ConA-stained oocyte treated with CK-666 and blebbistatin. Blue shows the Hoechst staining of chromatin. Frames are 34.5 s apart and movie length is 3825 s.

Supplementary Movie 14 Nocodazole blocks cortical cap contraction. Time-lapse imaging of a ConA-stained oocyte treated with CK-666 and nocodazole. Blue shows the Hoechst staining of chromatin. Frames are 34.5 s apart and movie length is 2035 s.

© 2011 Macmillan Publishers Limited. All rights reserved.